Tellus (1993), 45A, 493–510
Printed in Belgium – all rights reserved

TELLUS
ISSN 0280–6495

Linearization and adjoint of parameterized moist diabatic processes

By TOMISLAVA VUKIĆEVIĆ* and RONALD M. ERRICO, *National Center for Atmospheric Research*[1], *Boulder, CO 80307-3000, USA*

(Manuscript received 9 November 1992; in final form 22 April 1993)

ABSTRACT

The problems related to the development and applications of an adjoint model for a nonlinear model that has discontinuities in the governing equations are discussed in this study. We examine the hypothesis that a useful tangent linear model and its associated adjoint model can be developed for such a nonlinear model by using the reference state to determine the regimes associated with the discontinuities. Our nonlinear and linear experiments for the Pennsylvania State University/National Center for Atmospheric Research regional forecast model show that linearization of moist diabatic parameterizations is feasible using this method, but significant errors may be expected in the regions where transitions are frequent and associated with large tendency changes due to the model's moist diabatic parameterizations. We conclude that the tangent linear model and its associated adjoint model would be more accurate for a nonlinear model that has more well-behaved regime transitions. We suggest that nonlinear tests similar to the analysis shown in this study be performed prior to developing these linear models. If these tests show high nonlinearity due to regime transitions as a consequence of model deficiencies, we recommend first improving the nonlinear model before performing the linearization.

1. Introduction

Adjoints of atmospheric and oceanic models are used for various applications, such as variational data assimilation (Le Dimet and Talagrand, 1986; Thepaut and Moll, 1990; Zou et al., 1992, to mention some), inverse problems for ocean circulation (Tziperman and Thacker, 1989; Tziperman et al., 1993), evaluation of optimal growth rates of initial perturbations (Farrell, 1990; Tribbia and Baumhefner, 1991; Barkmeijer, 1992; Vukićević, 1993), sensitivity studies (Cacuci, 1981; Hall et al., 1982; Cacuci and Hall, 1984; Errico and Vukićević, 1992) and optimal parameter evaluation (Smedstad and O'Brien, 1991). Some of these applications consider sophisticated prognostic or diagnostic models, but most of the associated adjoint models do not include physical parameterizations that produce discontinuities in the model equations. Examples of these parameterized processes are moist convection, non-convective precipitation, radiative effects of clouds, and turbulent eddy fluxes.

The type of discontinuity in the formulation of each parameterization may vary greatly between models and the spatial resolutions at which they are applied. Since these parameterized processes may contribute significantly to the evolution of the model's solution, they should be included in the associated adjoint model (ADJM) for that model to provide the best possible information (see Errico and Vukićević (1992), for the interpretation of the ADJM solutions). Additionally, for many applications, including four-dimensional variational data assimilation, an adjoint for diabatic processes such as precipitation and cloud formulation may be necessary for the accurate analysis and consideration of moisture, radiation, and other fields.

[1] The National Center for Atmospheric Research is sponsored by the National Science Foundation.
* Corresponding author.

Adjoint development for models with discontinuities has been performed for a few models (e.g., Hall et al., 1982; Verlinde, 1992; Zou et al., 1993; Zupanski, 1993), but the limits of their applicability and the utility of their results, especially regarding limitations introduced by the discontinuities, have not been discussed in significant detail. In particular, although their adjoints produce correct (effectively linearized) results (aside from some approximations sometimes made), the ranges of applicability implied by the linearization remain unexamined or sometimes not even mentioned, except perhaps to note that the results are necessarily only locally applicable in model phase space (i.e., to infinitesimal or very small perturbations of model initial, boundary, or parameter specification). Most real applications of adjoint models require a not very local applicability of the results, however, and therefore the utility of even exact adjoint models that consider discontinuous or other highly nonlinear physics remains questionable.

The purpose of this study is to define general problems associated with the development of an adjoint for a model with discontinuities and to investigate possible solutions to these problems using a regional atmospheric forecast model (the Pennsylvania State University/National Center for Atmospheric Research (PSU/NCAR) mesoscale forecast model, designated MM4 and described by Anthes et al., 1987). Theoretical considerations are discussed in the next section. Some revealing analysis of the MM4 integrations is presented in Section 3. The linearization of parameterized moist diabatic processes for the MM4 model is discussed in Section 4, and the accuracy of this linearization is discussed in Section 5. An example of results produced using an ADJM is shown in Section 6. Conclusions and recommendations appear in Section 7.

2. Theoretical considerations

In this section we first define the main problems associated with the definition and development of an adjoint for a numerical model with discontinuities. Then we discuss possible solutions to this problem.

2.1. Statement of problem

As in Errico and Vukićević (1992), we consider the model in discrete form:

$$\boldsymbol{x}_{n+1} = \mathscr{M}(\boldsymbol{x}_n), \tag{1}$$

where $\boldsymbol{x}_n$ is the model state vector at time step n and $\mathscr{M}$ denotes the model operator. The components of the state vector are values of all prognostic model fields at all grid points (or for all coefficients if a spectral or finite-element model). This vector can also be augmented by boundary values or model parameters, but we will restrict discussion to the prognostic fields alone for which $\boldsymbol{x}_0$ denotes the initial conditions.

The tangent linear model (TLM) corresponding to (1) is

$$\boldsymbol{x}'_{n+1} = \boldsymbol{M}_n \boldsymbol{x}'_n, \tag{2}$$

where $\boldsymbol{x}'_n$ is an approximation to

$$\Delta \boldsymbol{x}_n = \boldsymbol{x}_n - \bar{\boldsymbol{x}}_n \tag{3}$$

interpreted as a perturbation about a time-dependent basic state, denoted by the overline, that is itself a solution to eq. (1), and $\boldsymbol{M}_n$ is the Jacobian matrix of the operator $\mathscr{M}$ evaluated for the state $\bar{\boldsymbol{x}}_n$. If $\mathscr{M}$ includes discontinuous functions, then some elements of $\boldsymbol{M}$ will not exist for some $\bar{\boldsymbol{x}}_n$, and even where elements of $\boldsymbol{M}$ do exist, they may do so only in a small neighborhood of $\bar{\boldsymbol{x}}_n$. In fact, some parameterization schemes act to push solutions toward, rather than away from, values where the Jacobian derivatives become nonexistent (e.g., convection schemes that adjust solutions to neutral stability).

The corresponding ADJM is

$$\frac{\partial J}{\partial \boldsymbol{x}_n} = \boldsymbol{M}_n^{\mathrm{T}} \frac{\partial J}{\partial \boldsymbol{x}_{n+1}}, \tag{4}$$

where J is a scalar measure of a forecast aspect that is a function of the forecast fields at some time (or times) (Errico and Vukićević, 1992) and superscript T denotes a transpose. In addition to the requirement that the elements of $\boldsymbol{M}$ exist, J must also be a continuous function of the forecast fields if $\partial J/\partial \boldsymbol{x}_0$ is to exist for all solutions to eq. (1). The latter requirement simply restricts the choices of J, but the former requirement suggests that problems may occur when some parameterization schemes are considered.

As an example of the problem posed by discontinuous forcing functions, consider the simple model:

$$x_{n+1} = \begin{cases} A(x_n) & \text{for } S(x_n) \geqslant 0 \\ B(x_n) & \text{for } S(x_n) < 0, \end{cases} \tag{5}$$

where here x is a scalar. A possible trajectory of x_n is shown by the heavy line in Fig. 1. If A and B are continuous functions of x, then a small perturbation of x_0 will result in a trajectory near the heavy line, unless it passes too near a point where $S = 0$. In the latter event, the condition in eq. (5) may change, and the trajectory may take a very different route (one of the dotted ones). Unfortunately, the route cannot be determined until the perturbation is specified.

In the context of the adjoint, each trajectory shown in Fig. 1 may be associated with a very different gradient $\partial J/\partial x_0$, so if the choice of trajectory is very sensitive to perturbations, a single gradient will not be a good description of the sensitivity unless we are interested in tiny (i.e., perhaps irrelevant) perturbations. A more global (and relevant) picture of the sensitivity would also require estimates of the sensitivity of all the conditions $S_n = S(x_n)$ encountered. In some simple variational problems of data fitting with few conditions, this is what is in effect determined (Bryson and Ho, 1975; Stengel, 1986). More generally, however, the number of possible trajectories to consider increases as s^n, where s is the number of branches

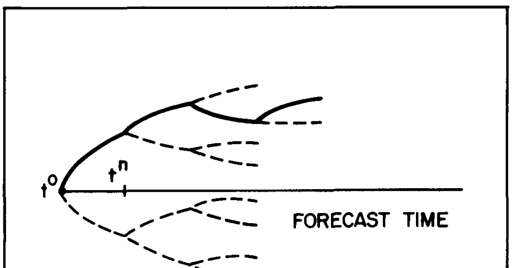

Fig. 1. Schematic representation of solution paths for a model that has discontinuities in the governing equations.

to consider at each time step. In a state-of-the-art numerical model, this number may be several times the number of grid point values, and even for a one-day forecast, n may be the order of 100 or much greater. Evaluation of global sensitivity is therefore prohibitive. Instead we must be content with evaluating local sensitivities (i.e., sensitivity to very small perturbations) and being aware that they may be so locally valid that their applications to problems considering significant perturbations may be inappropriate. In Subsection 2.2, we state some conditions under which single gradient may be more useful.

2.2. Conditions of reasonable accuracy

There are a number of conditions under which the TLM results and ADJM applications may be reasonably accurate even for significantly large perturbations (e.g., the size of errors in analyses produced by current data assimilation systems). It is difficult to express these conditions in mathematically precise terms that could easily be evaluated in a complicated models, such as used for numerical weather prediction. Yet, some guidance is required if we are to develop and use TLMs and ADJMs of these models. The conditions stated here are therefore applicable in this latter sense.

Also, it must be noted that the question of the applicability of the TLM or ADJM is not restricted to consideration of discontinuous forcing functions only, but actually depends on how strong all the nonlinearities are (i.e., the relative magnitudes of all the derivatives of $\mathscr{M}$ with respect to the state variables). In fact, the greatest inaccuracy of the moist version of our TLM derived from the MM4 was due to a model forcing term that is exponential, not discontinuous. That term is proportional to q^γ, where q is a specific humidity and $0 < \gamma < 1$ is a factor used for vertical interpolation. For values of q as small as 10^{-99} that occur in most solutions, the ratio of $\partial^2 q^\gamma/\partial^2 q$ to $\partial q^\gamma/\partial q$ becomes very large. Linearization about these values therefore described the evolution of perturbations so poorly that the TLM solutions were absurd. We reduced this problem by restricting $q = 10^{-8}$ to be the smallest value. This problem illustrates that it is not sufficient to simply perform an exact linearization of $\mathscr{M}$ to obtain a useful TLM.

If the continuous forcing terms in a model do not have strong nonlinearities (e.g., most of the advection terms are only quadratic in most models), then useful results may be obtained from its corresponding TLM or ADJM even when the original model has discontinuous forcing functions if some conditions are satisfied. These are:

Condition 1: The sensitivity of each conditional that determines solution branches (e.g., S in eq. (5)) with respect to small but finite-amplitude perturbations of the state vector is small when the state vector is not near critical values of the conditional. In eq. (5), this condition is that $\partial S/\partial x_n$ is small for all n when S_n is not near zero. This implies that perturbations do not change the sense of the conditionals except where the basic state trajectory lies close to critical points.

Condition 2: The trajectory does not pass near many critical values of the conditionals. In terms of an atmospheric model, this corresponds to the condition that most locations at most times are within a single regime and not close to transitions.

Condition 3: The occurrence of a regime transition does not imply a large change in forcing. This implies that regime transitions do not necessarily affect the forecast greatly, although it is unclear what their impact on perturbations themselves may be. Another way of stating this condition is that marginal states must have marginal impacts.

If these conditions are met, then we may expect that a linearization performed by specifying regimes according to the basic state conditions may be appropriate for finite-amplitude perturbation values.

An example of a parameterization that may satisfy the above conditions is the condensation and either cloud formation or rainout when the specific humidity exceeds a saturation threshold value q_s. Condition 1 is satisfied because the saturation condition depends on $\Delta q = q - q_s$, where neither q nor q_s change greatly for small changes of the state vector. Condition 1 is satisfied because, in a saturated environment, the amount of condensation is usually proportional to Δq which is linear with respect to q and well approximated by a linearization of q_s, and in a subsaturated environment the condensation is 0. Condition 2 is satisfied because in most cases, most areas are either dry or saturated for extended times (the periods depending on the scales modeled). The edges of storms are exceptions along with certain marginal shower cases. Condition 3 is satisfied, because if Δq is near zero, then any condensation is necessarily small also. An example of a parameterization that does not satisfy all these conditions will be presented in Section 3.

Another method for resolving the problem of treating linearization of model discontinuities was also examined recently (Verlinde, 1992). This method consists of eliminating discontinuities in the original nonlinear model without significantly impacting the original model solution. This is attempted by adding forcing terms that represent all possible regimes into the governing equations and assigning highly nonlinear but continuous weight functions to each of these terms. These weight functions are necessarily dependent on the state vector. The main advantage of this method over the first method is that the linearization problem is well posed because the discontinuities are actually eliminated. The main disadvantage of this method is that the changes to the original model equations are significant because one forcing term needs to be added for each S. Additionally, the number of numerical computations for the resulting modified model is much larger than for the original model because all possible regimes are represented for every model grid point and for all times in the forecast. We would like to point out that, although the model equations are continuous for this modified model, the linearization of the highly nonlinear weight functions may produce similar errors to the errors associated with marginal states described in the first method because for such weight functions, higher order derivatives may not be negligible.

3. Nonlinear tests

A test of the potential usefulness of TLM and ADJM results can be performed by first examining only nonlinear integrations. Here the nonlinear model considered is the version of the MM4 described in Errico and Vukićević (1992).

The usefulness of a linearization can be estimated by performing nonlinear integrations prior to constructing a TLM. Essentially, we examine whether perturbation solutions behave approximately linearly by examining three forecasts: a control and two perturbations. The perturbations are selected so that x'_0 of one is some factor $-2 < r < 2$ of the other; i.e., the perturbations have identical structures but slightly different amplitudes. If the perturbations behave quasi-linearly in the forecast, then the perturbations should scale the same at all forecast times as they do initially. This is a more stringent test than simply examining the ratio of the L2 norms (i.e., the square roots of the sums of the squares of all the components) of the two x'_0, which should also be asymptotic to r as both norms tend to zero, since our test is applied to each vector component individually.

Of course, the ratio of every corresponding component of the two x_n will not equal r, nor even be necessarily near r. For this reason we restrict attention to qualitative comparison of contour plots of selected corresponding fields for pairs of perturbations.

We examined r for a case of Atlantic explosive cyclogenesis during the 12-h period prior to 0000 UTC 15 February 1982. This case was selected because the forecast is strongly affected by moist diabatic (discontinuously parameterized) processes, yet the regime selection in most locations was not expected to be sensitive to moderately-sized perturbations (since the dynamics producing the precipitation are both strong and localized). The sea level pressure forecast produced by the MM4 for the end of the forecast (denoted hereafter as the verification time) is shown in Fig. 2. There is

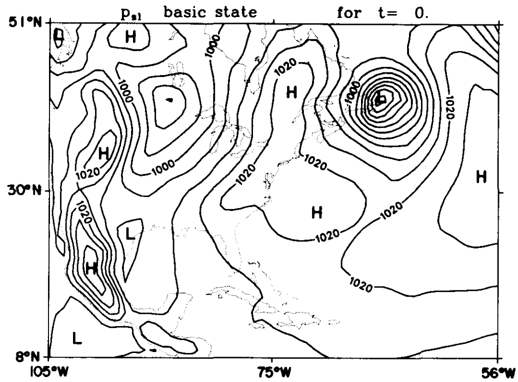

Fig. 2. Sea level pressure forecast verifying at 0000 UTC 15 February 1982. Contour interval is 5 mb.

a deep cyclone centered south of Nova Scotia. The MM4 shows good skill in predicting the development of this cyclone (Kuo and Low-Nam, 1990).

For the first initial perturbation we used the difference between two 36 h MM4 forecasts originating from slightly different initial conditions valid at 1200 UTC 13 February 1982. The initial difference between those forecasts is determined by uniformly distributed random perturbations of the model fields, but after 36 h, the various fields are correlated between each other and in space due to action by the model dynamics. These correlated differences are used for our experiment because

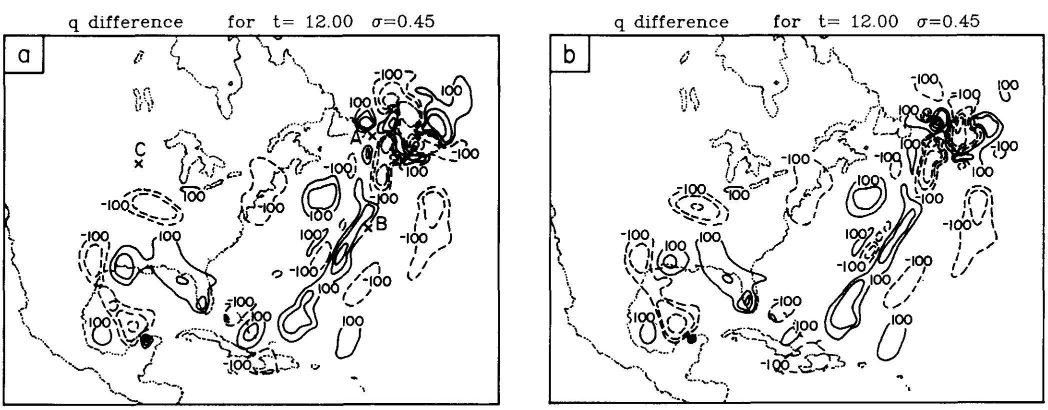

Fig. 3. Mid-level ($\sigma = 0.45$) specific humidity differences between the control and perturbed forecasts for 12-h integration for the case with: (a) initial perturbation x'_1 and (b) initial perturbation $x'_2 = \frac{1}{2}x'_1$. Physical units are 10^{-8} g kg^{-1}. Contours are unevenly spaced in both figures but each contour interval in (a) is two times that of the corresponding interval used in (b). Consequently, similarity in patterns between (a) and (b) indicates that the criterion for linearization is satisfied ($r^n \simeq r^0$). The opposite conclusion applies for the regions where the patterns are not similar.

Tellus A/45/5-11

they are free from the initial unforced gravity waves and are diffusion adjusted (Errico, 1990). The amplitude of x'_0 chosen was well within the linear range according to the results for the dry version of MM4 (Errico et al., 1993a, hereafter referred to as EVR93). For example, the sea level pressure perturbations are on the order of 0.01 mb. These perturbation amplitudes are much smaller than typical analysis errors, but more realistic initial perturbations are used for experiments discussed later in this section.

A value of $r = 2$ was used for our test. We will use subscripts 1 and 2 to the two perturbations when it is clear the time index n is not intended. Fields of q' at the verification time for the two perturbations are displayed in Fig. 3. The magnitude of q'_1 is twice that of q'_2 through most of the domain. This ratio is not realized mainly within and near the Atlantic cyclone and near some locations along its associated cold frontal zone. These are the same regions where precipitation occurs. This result suggests that applications of a corresponding TLM or ADJM may be inaccurate in these regions for perturbations even this small, most likely because of the discontinuities associated with the parameterized moist physics.

In order to identify the discontinuities in the model that are associated with these processes, we analyzed time series of $\partial q/\partial t$ (hereafter referred to as QT) and for the terms in the moist model equation that contribute to this time tendency. These time series are produced for several model grid

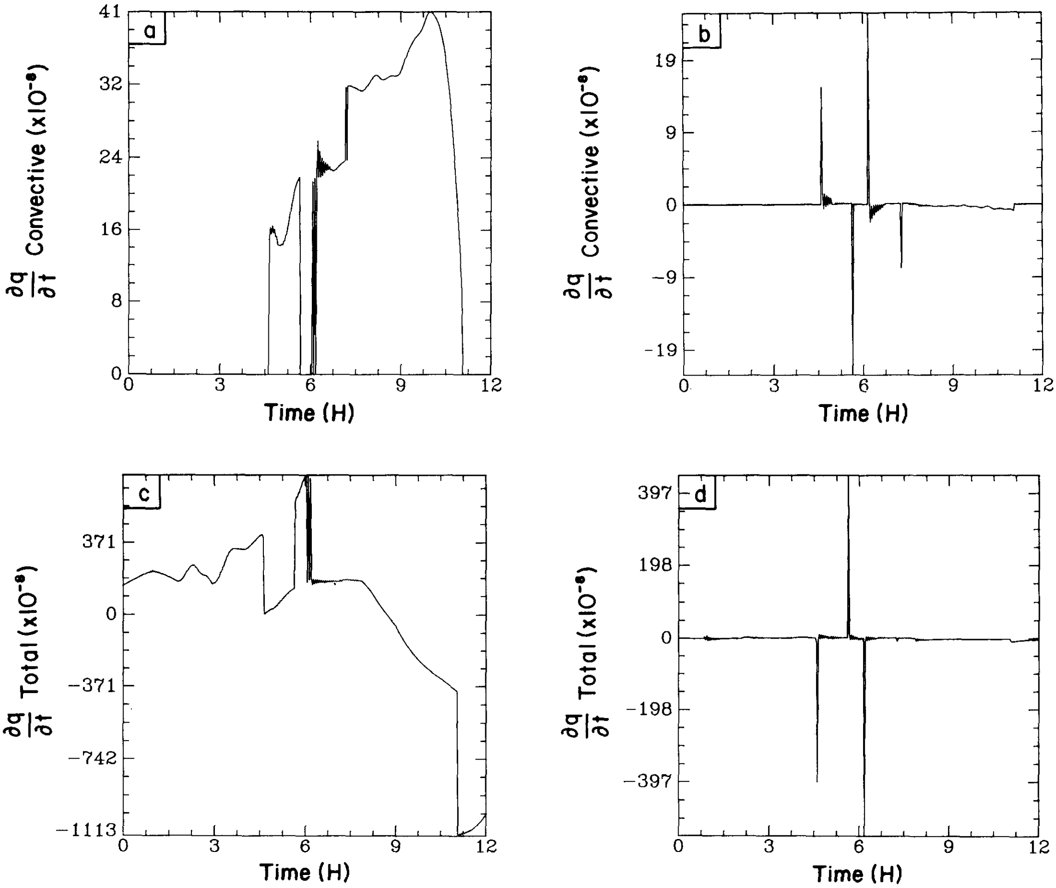

Fig. 4. Time series of CT and QT for grid point (B) for: the control nonlinear integration (panels a and c) and the difference between the control and perturbed integration for the small amplitude initial perturbation (panels b and d).

points that represent different types of evolution such as: (1) evolution with only a few transitions between precipitating and non-precipitating regimes, (2) evolution with repeated transitions between these two regimes, and (3) evolution without any precipitation. Values for these time series are provided at every time step throughout the 12-h integration. We only specifically present the time series of QT and the contributions from the convection (CT) for three grid points marked (A), (B), and (C) in Fig. 3a. Point (A) is located in the main storm region, point (B) is in the explosive cyclone frontal zone, and point (C) is located west of the Great Lakes. This latter location is far away from the main storm and is characterized by calm weather for the period considered in our study. All three points are located at the mid-tropospheric level in the model.

The time series for CT and QT for point (B) are shown in Figs. 4a, c, respectively. The values for CT (Fig. 4a) are equal to zero for the periods without convection. Fig. 4a shows four occurrences of regime transition at about 4.5, 5.7, 6.0, and 11.1 h of integration. The initial period without convection is 4.5 h long after which the convection is turned on and lasts for about 1.2 h. A short (0.3 h) period without convection follows. Then the convection is turned on again and persists for about 5 h. The evolution of QT (Fig. 4c) suggests that its forcing is discontinuous.

To estimate sensitivity of the model to the initial perturbations for the transition times and within each of the regimes, we compute the time series of QT and CT for the differences between the control MM4 integration ($\bar{x}_n$) and the perturbed integration (x_n). First we notice that for every regime

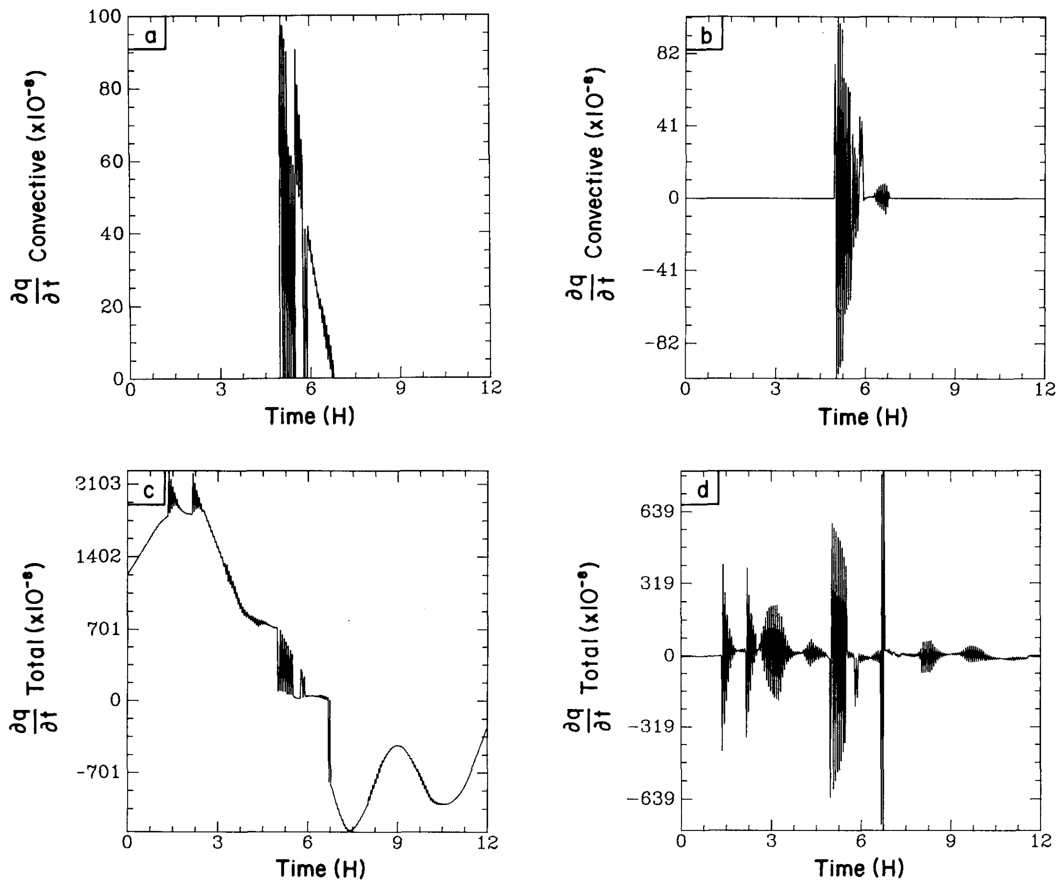

Fig. 5. As for Fig. 4 but for grid point (A).

transition in the control integration the perturbation values of CT and QT (Figs. 4b, d) have peak amplitudes that are of the same order of magnitude as the control amplitudes. Detailed examination of the evolution around these transition points shows that these large differences between the control and perturbed integrations occur within only two time steps of the model. For the remaining periods (99% of integration time), the perturbation amplitudes are very small as expected for the small initial perturbations. We conclude that for the type of evolution that characterizes grid point (B), linearization may be accurate for significant perturbations.

The second point that we analyze (A) represents different evolution than that at point (B). The control values of CT and QT are shown in Figs. 5a, c, respectively, for this point. The convection occurs for the first time at about 4.8 h of integration (Fig. 5a). Unlike for point (B), the convection occurrence after this time is characterized by $2\,\Delta t$ oscillations, where Δt is the model time step. Only around forecast times 5.6 h and 6.5 h does the convection remain turned on continuously for short periods of time. The convection terminates at about 6.75 h. The time series for the total tendency (QT) shows discontinuities during the convective period that are also characterized by $2\,\Delta t$ oscillations (Fig. 5c). Moreover, these high frequency oscillations also occur at other times in the forecast, such as around 1.5 h, 3.25 h, and 9.0 h. These features are not directly related to the convective activity in point (A), but may be caused by $2\,\Delta t$ oscillations at other points. The cause of these oscillations in the MM4 is not clear, but further examination has revealed several oscillations of model conditionals, including oscillations due to interactions between different parameterizations (in particular, the convection and non-convection schemes). Further analysis of these oscillations was considered beyond the intention of our study. We discuss possible ways to avoid these oscillations in the following sections. To our knowledge this feature of the MM4 solution has not been revealed before.

The differences between the control time series and the time series for the perturbed MM4 integration are presented in Figs. 5b, d for point (A). During the convective period these differences are also characterized by $2\,\Delta t$ oscillations (Fig. 5b). The amplitude of perturbation CT is approximately twice that of the control amplitude throughout the period with "turn-on-turn-off" convection. This amplitude becomes small for the short periods with persisting convection. The perturbation amplitudes are large for the former period because the perturbed integration is phase shifted with respect to the control integration by only one time step. The time evolution of perturbation QT shows (Fig. 5d) that the large amplitudes occur for all periods characterized by $2\,\Delta t$ oscillations. The remaining periods have small perturbation amplitudes as expected for the small initial perturbation. We conclude that for the type of evolution observed at grid point (A), the linearization may be inaccurate even for small perturbations. In the next section we suggest one possible way to overcome this difficulty.

Grid point (C) is characterized by the absence of convection or large-scale precipitation. Also, the oscillations with $2\,\Delta t$ frequency do not occur at this point (Fig. 6). The evolution of QT for the control integration is rather smooth (Fig. 6a). The amplitudes of perturbation QT (Fig. 6b) are almost three orders of magnitude smaller than the control values. This conclusion applies also for the perturbations associated with those forecast periods without regime transitions or $2\,\Delta t$ oscillations for points (A) and (B).

We also perform time series analysis for perturbations with more realistic initial amplitudes. The structure of these perturbation fields are the same as for the previous experiment, but the associated amplitudes are about $60\times$ larger. The regime transition points are sensitive to this initial perturbation as for the perturbations with small amplitudes. The amplitudes of perturbation CT are larger for the larger initial perturbation as expected. The main difference between the small and this more realistic perturbation case is that the convection continues throughout the forecast period 5.7–6.0 h for the latter case due to the larger initial amplitude. The evolution of this perturbation QT shows the discontinuities for the same forecast times as the small perturbation integration.

For the realistic perturbation, the time series for point (A) are different than for point (B), as for the weaker perturbation. The perturbation values of CT for this point have large amplitudes and $2\,\Delta t$ oscillations around 2.25 h and 3.8 h of forecast unlike the small perturbation CT. These latter per-

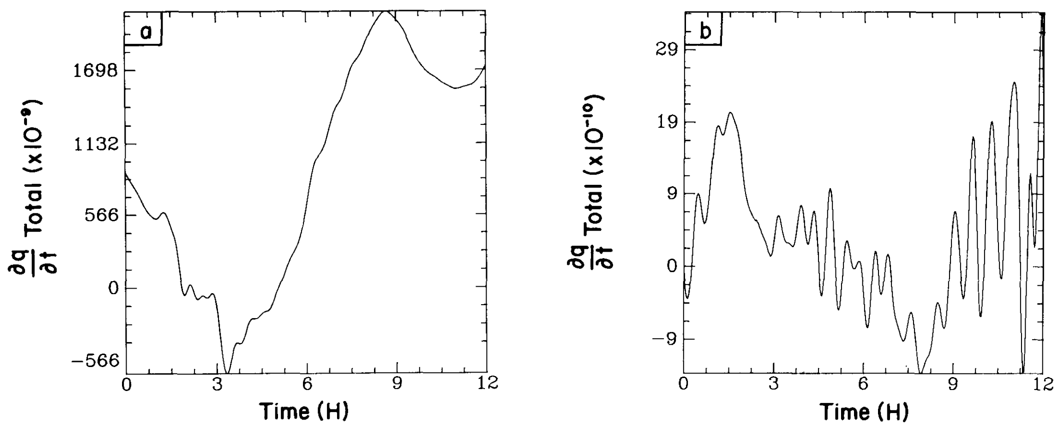

Fig. 6. Time series of QT for grid point (C) for: the control nonlinear integration (panel a) and the difference between the control and perturbed integration for the small amplitude initial perturbation (panel b).

turbations have zero values for these times. It is important to notice that the amplitudes of perturbation CT for both small and large initial perturbations are of similar magnitude for point (A). This feature characterizes also the time series for QT. This conclusion does not apply to points (B) and (C). For these points the small amplitude perturbations are about 60 times smaller than the perturbations associated with the larger initial perturbation. This relation is expected for the linear or approximately linear evolution. These results suggest that the $2\,\Delta t$ oscillations trigger highly nonlinear behavior in the model convective parameterization and related schemes for certain marginal precipitation states similar to the state in point (A).

It is interesting to note that this nonlinearity forces gravity waves in the perturbation fields. This is readily observed in the perturbation sea level pressure field for the case with small amplitude initial perturbation (Fig. 7a). The equivalent field for the integration with larger amplitude initial perturbation does not have this gravity wave signature (Fig. 7b). This result suggests that for very small perturbations, the dominant mechanism of perturbation evolution is the forcing

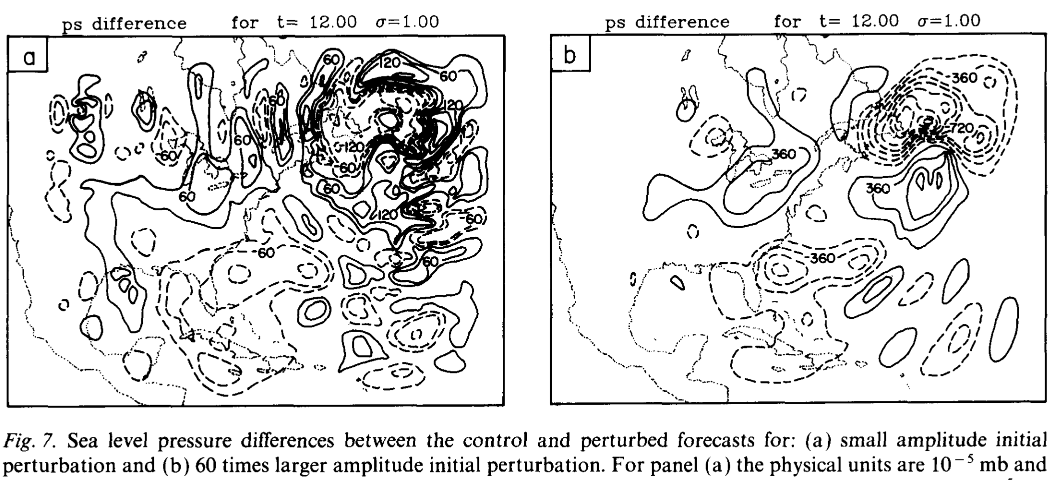

Fig. 7. Sea level pressure differences between the control and perturbed forecasts for: (a) small amplitude initial perturbation and (b) 60 times larger amplitude initial perturbation. For panel (a) the physical units are 10^{-5} mb and contour levels are: ± 30, ± 60, ± 120, ± 180, ± 300, ± 600, and ± 1200. For panel (b) the physical units are 10^{-5} mb and contour levels are evenly spaced with the interval 180.

of the gravity waves for the regions and periods where the convection is sensitive to $2\,\Delta t$ oscillations. This region is associated with the core of the cyclone for the synoptic case used in this study.

The results presented in this section indicate that the linearization of the moist diabatic MM4 is possible based on the method given in Subsection 2.2, but the TLM may be erroneous for the regions where the oscillations with $2\,\Delta t$ frequency are dominant. The linearization of moist diabatic processes for MM4 is described in the next section. The accuracy tests for the TLM that includes these processes are presented in Section 5.

4. Linearization of moist processes in MM4

The physical parameterizations that produce discontinuities in the MM4 are: (1) Kuo-Anthes cumulus parameterization, (2) large-scale precipitation, (3) effects of clouds on surface radiation, and (4) vertical momentum mixing and heat flux parameterizations. The linearization of (4) is described in EVR93 for the dry version of the MM4. In this section we describe linearization of (1), (2), and (3).

4.1. *Cumulus parameterization and large-scale precipitation*

The Kuo-Anthes cumulus parameterization used in the MM4 is based on the schemes described in Kuo (1974) and Anthes (1977). For this parameterization the vertically integrated moisture convergence determines the condensation and moistening rates. The condensation produced heating is distributed vertically using a parabolic function (Anthes et al., 1987). The associated moistening of the column is performed using a vertical profile dependent on the normalized supersaturation amount. The vertical eddy-flux divergence of water vapor associated with convection is also considered. The contributions to the thermodynamic equation and the moisture tendency equation for this parameterization are given by the following expressions:

$$\left(\frac{\partial p^*T}{\partial t}\right)_{\rm c}=\frac{L_{\rm v}}{C_{\rm pm}}N_{\rm h}(\sigma)(1-b)\,M_{\rm t}, \tag{5}$$

$$\left(\frac{\partial p^*q}{\partial t}\right)_{\rm c}=bM_{\rm t}N_{\rm m}(\sigma)+V_{\rm qf}(\sigma), \tag{6}$$

$$b=\begin{cases}2(1-{\rm RHA}) & \text{for}\quad {\rm RHA}\geqslant 0.5,\\ 1 & \text{for}\quad {\rm RHA}<0.5,\end{cases}$$

$${\rm RHA}=\int_0^1\frac{q}{q_{\rm s}}\,d\sigma,$$

where $M_{\rm t}$ is the vertically integrated moisture convergence, b is the fraction of precipitated moisture, and $N_{\rm h}$ and $N_{\rm m}$ are vertical profiles of heating and moistening, respectively. $V_{\rm qf}$ is the vertical integral of the eddy-flux divergence. Remaining variables and constants are:

σ-model vertical coordinate

p^*-surface pressure minus model top level pressure

q-specific humidity

$q_{\rm s}$-saturation specific humidity

T-temperature

$C_{\rm pm}$-specific heat at constant pressure

$L_{\rm v}$-latent heat of condensation

$\left(\frac{\partial p^*T}{\partial t}\right)_{\rm c}$-contribution to total tendency for p^*T by convection

$\left(\frac{\partial p^*q}{\partial t}\right)_{\rm c}$-contribution to total tendency for p^*q by convection

The large-scale precipitation is parameterized in the MM4 as the excess moisture with respect to the supersaturation. For this scheme the specific humidity is corrected to supersaturation, and the temperature is increased due to associated latent heat release. This is expressed by:

$$q_{\rm cor}=q-\Delta q, \tag{7}$$

$$T_{\rm cor}=T+\frac{L_{\rm v}}{C_{\rm pm}}\Delta q,$$

where

$$\Delta q = \begin{cases} r(q-q_s) & q \geqslant q_s \\ 0 & q < q_s, \end{cases}$$

$$r = \left[\frac{1+L_v^2 q_s}{R_v C_{pm} T^2}\right]^{-1}.$$

The linear equations equivalent to eqs. (5), (6), and (7) are:

$$\frac{\partial (p^* T)'}{\partial t} = H\left(\frac{L_v'}{\bar{L}_v} - \frac{b'}{(1-\bar{b})} + \frac{M_t'}{\bar{M}_t} - \frac{C_{pm}'}{\overline{C_{pm}}}\right), \quad (8)$$

$$\frac{\partial (p^* q)'}{\partial t} = M\left(\frac{b'}{\bar{b}} + \frac{M_t'}{\bar{M}_t} - \frac{N_m'(\sigma)}{\bar{N}_m \sigma}\right) + V_{qf}'(\sigma), \quad (9)$$

$$b' = \begin{cases} -2\int_0^1 \frac{\bar{q}}{\bar{q}_s}\left(\frac{q'}{\bar{q}} - \frac{q_s'}{\bar{q}_s}\right) d\sigma & \text{for RHA} \geqslant 0.5 \\ 0 & \text{for RHA} < 0.5, \end{cases} \quad (10)$$

$$M_t' = -m^2 g^{-1} \int_0^1 \nabla \frac{(p^* \mathbf{v})' \bar{q} + \overline{(p^* \mathbf{v})}\, q'}{m} d\sigma, \quad (11)$$

$$N_m' = \frac{\bar{q}_s - \bar{q}}{\int_{\sigma_{KTOP}}^1 (\bar{q}_s - \bar{q})\, d\sigma} \times \left(\frac{q_s' - q'}{\bar{q}_s - \bar{q}} - \frac{\int_{\sigma_{KTOP}}^1 (q_r' - q')\, d\sigma}{\int_{\sigma_{KTOP}}^1 (\bar{q}_s - \bar{q})\, d\sigma}\right), \quad (12)$$

$$V_{qf}' = \frac{(1-\bar{b})\, q \bar{M}_t}{4.3 \times 10^{-3}} \left[-\overline{p^*} \frac{\partial}{\partial \sigma} (\dot{\sigma}_c (\bar{q}_c - \bar{q}))\right] \times \left[-\frac{b'}{1-\bar{b}} + \frac{M_t'}{\bar{M}_t} - \frac{(p^*)'}{\overline{p^*}} - \frac{\partial}{\partial \sigma} \times \left(\frac{(\dot{\sigma}_c)'}{\overline{\dot{\sigma}_c}} + \frac{q_c' - q'}{\bar{q}_c - \bar{q}}\right)\right], \quad (13)$$

where

$$H \equiv \frac{\overline{L_v}}{\overline{C_{pm}}} (1-\bar{b})\, \bar{N}_h(\sigma)\, \bar{M}_t,$$

$$M \equiv \bar{b} \bar{M}_t \bar{N}_m(\sigma),$$

$$q_{cor}' = q' - \Delta q',$$

$$T_{cor}' = T' + \frac{L_v'}{\overline{C_{pm}}} \overline{\Delta q} + \frac{\overline{L_v}}{\overline{C_{pm}}} \Delta q' - \frac{L_v'}{(\overline{C_{pm}})^2} \overline{\Delta q}\, C_{pm}',$$

$$\Delta q' = \begin{cases} \bar{r}(q' - q_s') & \bar{q} \geqslant \overline{q_s} \\ 0 & \bar{q} < \overline{q_s}. \end{cases} \quad (14)$$

The barred variables represent the basic state (i.e., reference state produced by the MM4), and primed variables represent perturbations to this basic state. σ_c is the vertical velocity within cloud, q_c is the cloud specific humidity, and m is the projection scale factor for the Lambert conformal projection used in MM4.

4.2. *Radiative effects of moisture*

Perturbations of moisture effect the radiative fluxes at the ground by affecting both the column integrated precipitable water W and the cloud fractions η_i that is defined for three levels (denoted as high, medium, and low or by $i = 1, 2, 3$, respectively). The latter affects both downward long wave and solar radiation.

Since W is an expression linear in $p^* q$, it poses no problems for the TLM except that, for the radiation calculation, any $W < 0.1$ cm is replaced by the value 0.1 cm. The TLM treats this condition simply by setting $W' = 0$ if $\bar{W} = 0.1$ cm.

Each cloud fraction is computed as a linear function of the maximum relative humidity (r_H) computed for the σ-levels that fall within the layer for which the cloud is defined. In the TLM, perturbations of each cloud fraction are determined from the linearized r_H' for the level at which $\overline{r_H}$ is a maximum, since $1 \leqslant \eta_i \leqslant 0$, η_i' is set to 0 whenever $\overline{\eta_i}$ is either 1 or 0.

The downward long wave radiation is computed as

$$I_\downarrow = d_c \varepsilon_a \sigma_{SB} T_a^4, \quad (15)$$

where ε_a is an atmospheric long-wave emmisivity that is a function of W, d_c is an enhancement factor due to clouds (determined as a linear function of the three cloud fractions), σ_{SB} is the Stefan-Boltzmann constant, and T_a is the air temperature at the first level greater than 40 HPa above the surface. The factor $d_c \varepsilon_a$ is restricted to be not greater than 1. The TLM linearization for $I_\downarrow$ is, therefore,

$$I'_\downarrow = \begin{cases} \overline{I_\downarrow}\left(\dfrac{d'_c}{\overline{d_c}} + \dfrac{\varepsilon'_a}{\overline{\varepsilon_a}} + \dfrac{4T'_a}{\overline{T_a}}\right) & \text{for} \quad \overline{d_c \varepsilon_a} < 1, \\ 4\overline{I_\downarrow}\dfrac{T'_a}{\overline{T_a}} & \text{for} \quad \overline{d_c \varepsilon_a} = 1. \end{cases} \tag{16}$$

The clear-air transmissivities and backscattering coefficients in the MM4 are interpolated from values in a look-up table as a function of path length and W. Transmissivities are then adjusted for the surface pressure. The effects of perturbations of these variables on the perturbed solar flux at the surface is almost always only a few % of the effect of other perturbations even for perturbations of T, p_s, and q twice the magnitude of current analysis uncertainties. Perturbations of these transmissivities and coefficients, therefore, are not considered by the TLM to simplify the formulation and software.

Perturbations of the short-wave cloud absorption (τ_{ac}) and scattering (τ_{sc}) transmissivities are determined from η'_1, η'_2, and η'_3. The gradient of the short-wave irradiance Q_s with respect to both τ_{ac} and τ_{sc} is determined so that

$$Q'_s = \frac{\partial Q_s}{\partial \tau_{ac}} \tau'_{ac} + \frac{\partial Q_s}{\partial \tau_{sc}} \tau'_{sc}. \tag{17}$$

In summary, there are 11 switches (3 regarding levels of maximum r_H, 6 regarding bounds on η, and 2 regarding bounds on W and $d_c \varepsilon_a$) that are specified according to their basic state values. Perturbations of the table look-up variables are ignored.

Expressions (8–17) describe the moist diabatic equations for the TLM in continuous form. The actual TLM in discrete form is an exact linearization of the complete discretized MM4 (see also EVR93). The basic state used for the linear integrations is defined by a sequence of state vectors produced by the nonlinear MM4 forecast. This sequence has an associated update period (EVR93). The linear coefficients in the TLM are changed abruptly during the integration at equally spaced intervals defined by this update period with the exception of the coefficients associated with the parameterized convection and large-scale precipitation. These coefficients are computed as the time average over the update period. This averaging is performed to minimize the errors caused by the numerical oscillations with $2\,\Delta t$ frequency. Consequently, the minimum basic state update period used for the TLM integrations in this study is $2\,\Delta t$.

5. Accuracy of moist TLM

The accuracy of our TLM is tested in order to understand the accuracy of its corresponding adjoint because the accuracies of both are identical. Additionally, the accuracy of the ADJM itself can be viewed as a degree of confidence associated with this model solution for the given application. This approach is used in the next section where our ADJM is applied to a sensitivity experiment.

We consider two types of accuracy for the TLM: (1) the accuracy of perturbation time tendencies at some single time and (2) the accuracy of time integration. The dry experiments (EVR93) demonstrate very high accuracy for (1). For perturbation magnitudes as large as analysis uncertainties, the correlation (CC) between the TLM produced time tendency and the nonlinear perturbation time tendencies for the dry experiments is $CC > 0.999$ for the winter case that is considered in that study. The time integration accuracy is also high for the dry cases. For example, $CC = 0.96$ for the basic state update period as long as 30 min and for 72-h integration periods.

The first type of accuracy is more difficult to test for the TLM with moist processes because it is not straightforward to select the basic state that includes all possible regimes allowed in the model parameterizations within this domain. To avoid this situation, we have tested the accuracy of time tendencies for each physical regime individually for selected grid points. These tests show high accuracy similar to the dry cases.

The time integration accuracy is evaluated using 12-h integration of the explosive cyclone case. The TLM solution is obtained using the basic state with the update period of $2\,\Delta t$ and the initial perturbation equal to the larger perturbation used in the experiments in Section 3. This solution is compared with the nonlinear perturbation defined as before by

$$\Delta \boldsymbol{x}_n = \boldsymbol{x}_n - \bar{\boldsymbol{x}}_n.$$

The measure of accuracy that we consider are the point differences between the nonlinear and linear perturbation solutions (hereafter referred to as TLM errors). These errors are shown in Figs. 8a, 9a, and 10a for the perturbation zonal wind component (u), temperature (T), and the specific humidity (q), respectively, for a mid-tropospheric model level. The equivalent nonlinear perturbation fields are also displayed for comparison in Figs. 8b, 9b, and 10b, respectively. The TLM errors for u and T are very small everywhere in the domain except near the cyclone center. In this region the TLM errors are as large as the nonlinear perturbations. It is interesting to note that the latter perturbations have largest amplitudes in this region also. This result suggests that the TLM errors reach maximum values when the nonlinear perturbation values are large due to the parameterized moist processes. This conclusion applies for the short integration period that is used in our experiment. For the longer periods, the second order nonlinear interactions may become more important than the higher order nonlinear interactions that are associated with the moist parameterizations. This is because the second order nonlinear interactions occur everywhere in the domain and at all times, unlike the latter processes.

The TLM errors and the nonlinear perturbations for the specific humidity field are shown in Fig. 10. Similar to the errors for u and T perturbations, the relative TLM errors for this field are large in the explosive cyclone. Unlike for the former perturbations, significant errors also occur at some locations along the main frontal zone associated with this cyclone. Additionally, the TLM errors for q are largest for the highest model levels (not displayed). This is because in the MM4 the contributions from the vertical and horizontal advection are not considered for the horizontal grid points that have convection, and the contribution CQ is typically zero for these levels (see Section 3 for the definition of CQ and QT). Consequently, QT is highly discontinuous for these points, and the TLM errors that originate from the high frequency numerical oscillations are dominating the perturbation solution for the highest model levels, although the convection does not occur at these levels.

It is clear from these results that the specific humidity perturbations are most directly affected by the inherent linearization errors that are associated with the discontinuities in the moist parameterizations. We would like to emphasize that the numerical deficiency of the MM4 that is characterized by $2\,\Delta t$ oscillations in the convection parameterization and in the related schemes (i.e., large-scale precipitation) contributes most to these errors. The time average coefficients that are used for the convection and the large-scale precipitation portion of the TLM improve this model performance with respect to the integrations with the coefficients that are updated abruptly, but do not eliminate these TLM errors. We believe that improvements to the model numerical schemes and/or physical parameterizations in the nonlinear

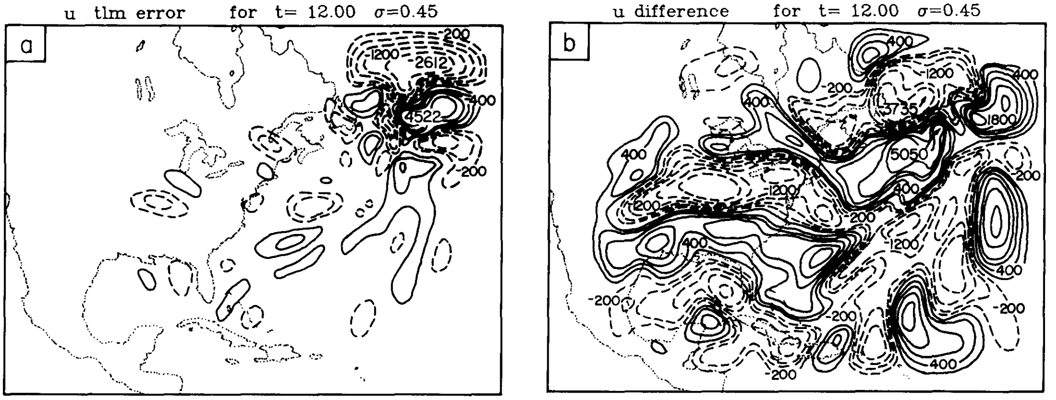

Fig. 8. Zonal wind component for model level $\sigma = 0.45$ and 12 h integration for: (a) TLM error and (b) nonlinear perturbation. Physical units are $10^{-3}\ \mathrm{ms}^{-1}$.

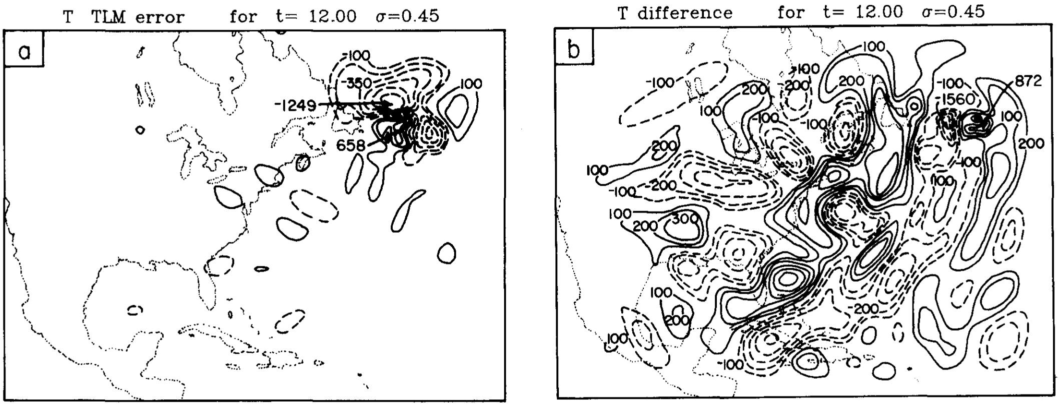

Fig. 9. As for Fig. 8, but for temperature. Physical units are 10^{-3} K.

model would also improve the accuracy of the associated TLM. Consequently, the adjoint model that is the exact adjoint for the given TLM also would have higher accuracy.

As an example, we have performed the same nonlinear tests that are described in Section 3 for the regional climate model that is based on the MM4 (Giorgi and Marinucci, 1991). This model has some numerical features and physical parameterizations different from the MM4 that is used in our study. Our time series analyses show that this regional climate model does not produce high frequency oscillations associated with the convective parameterization and related schemes. Based on this result and the results shown in Sections 3 and 4, we conclude that improved parameterizations and the time differencing scheme used in the regional climate model would cause smaller errors in the TLM and, consequently, the associated adjoint model would be more accurate.

We would like to point out that the adjoint model inaccuracies originating from the discontinuities in the original nonlinear model may present bigger problems for the applications involving use of the adjoint for the model sensitivity evaluation than for the applications, such as the variational data assimilation and optimal parameter evaluation. This is because the optimization procedure involves successive corrections for the control variables using pairs of nonlinear and adjoint model integrations in an iterative fashion. Additionally, the optimal solution is sought for the given reference state (e.g., observations), and as

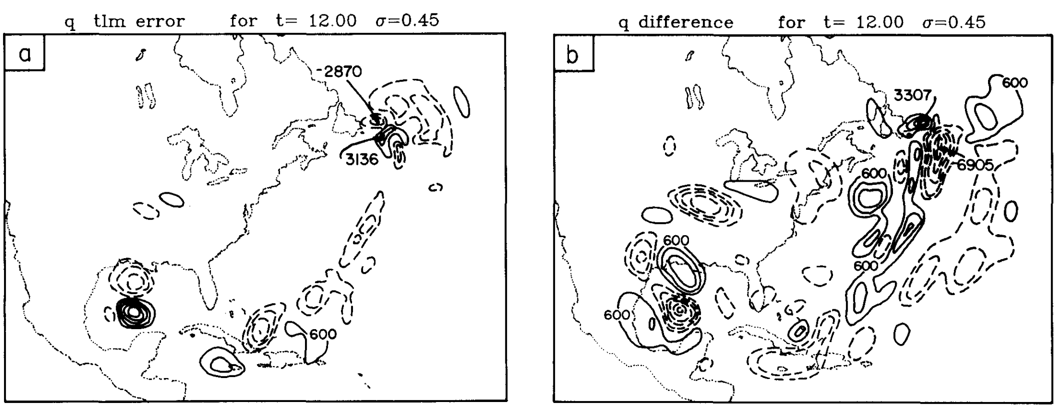

Fig. 10. As for Fig. 8, but for specific humidity. Physical units are 10^{-7} g kg^{-1}.

long as this state provides sufficient information for the regime transitions, the convergence of the optimization procedure can be controlled using the appropriate kind of penalty function. Examples of this approach are given in the literature on the optimal control theory for simpler models (Bryson and Ho, 1975; Stengel, 1986; Miller et al., 1993). For the sensitivity study purposes, the inherent uncertainties in the adjoint model may produce misleading results for the models with large sensitivity of the regime transitions to the small changes in the input vector. In the next Section we present a simple sensitivity test using our adjoint model solution. This test is performed to evaluate the reliability of this adjoint model for this application.

6. ADJM reliability test

The adjoint model for the dry version of MM4 (Errico et al., 1993b) has been developed following the procedure described in Errico and Vukićević (1992). The adjoint for the moist diabatic portion of the TLM is produced in this study in the same fashion as the dry adjoint. Consequently, the complete adjoint for the MM4 is the exact adjoint for the complete TLM that is used for the results shown in the previous section.

The sensitivity of a forecast aspect $J(\boldsymbol{x}_n)$ to the perturbations in the initial conditions $(\boldsymbol{x}'_0)$ is approximately given by the solution of the adjoint model. Consequently, knowledge of this solution should be sufficient for the evaluation of the change of J due to an arbitrary given small amplitude perturbation $\boldsymbol{x}'_0$ using

$$\Delta J^n_{\mathrm{L}} = \frac{\partial J^n}{\partial \boldsymbol{x}_0} \boldsymbol{x}'_0,$$

where n is the time index, as before, and subscript L stands for the "linear model." This expression represents a first order Taylor series approximation to the actual change of J (Errico and Vukićević, 1992). The actual change is given by the nonlinear model solutions using

$$\Delta J^n_{\mathrm{N}} = J^n(\boldsymbol{x}_n) - J^n(\bar{\boldsymbol{x}}_n),$$

where $\boldsymbol{x}_n = \mathcal{M}(\boldsymbol{x}_0 + \boldsymbol{x}'_0)$ and $\bar{\boldsymbol{x}}_n = \mathcal{M}(\boldsymbol{x}_0)$, as before, and subscript N stands for the "nonlinear model." The difference between ΔJ^n_{L} and ΔJ^n_{N} shows the degree of reliability associated with the adjoint model solution.

For our test, we consider the forecast aspect that represents the weighted average of surface pressure (p_{s}) in the local region centered at the explosive cyclone center for the forecast time shown in Fig. 2. The weights that are used for J are given by

$$w_{ij} = \cos[(i - ic)^2 + (j - jc)^2],$$

where i and j are zonal and meridional grid point indices, respectively, and ic and jc denote the center of the local region of interest. The starting value for the adjoint integration is given by $(\partial J^n/\partial p_{\mathrm{s}}) = w_{ij}$ (Fig. 11a). The adjoint model solution for 12 h prior to this verification time (i.e., initial forecast time) is shown in Fig. 11b for the specific humidity field $(\partial J^n/\partial q_0)$. The maximum amplitudes for this quantity are located near the cyclone center at this time, which is approximately 800 km southwest from the cyclone center at the verification time. The values of $\partial J^n/\partial q_0$ are one order of magnitude smaller than these maximum values elsewhere in the domain. This result suggests that the mid-tropospheric moisture associated with the cyclone at the initial time is important for this cyclone surface pressure forecast 12 h later. Other adjoint solution fields, such as $\partial J^n/\partial T_0$ and $\partial J^n/\partial p_{\mathrm{s}0}$ (not displayed), have maximum amplitudes also associated with the initial cyclone. Additionally, these fields have significant amplitudes in the regions remote from this cyclone. These amplitudes are associated with a gravity wave sensitivity pattern similar to the results shown in Errico and Vukićević (1992) for dry cases. The latter results, however, have the gravity wave sensitivity patterns at periods shorter than 6 h, unlike the current result that shows the gravity wave pattern is still present at 12 h prior to the verification time. These differences suggest that the gravity wave sensitivity for the moist cases may be present at any time in the forecast due to the forced gravity waves associated with convection. It is not clear whether these results are an artifact of the inherent inaccuracies that are discussed in Section 5, or whether they represent the actual properties of the moist diabatic processes in our forecast model. This problem will be treated in future studies.

The values of ΔJ^n_{L} and ΔJ^n_{N} are 3.603×10^{-2} and 1.905×10^{-2} for the small amplitude initial

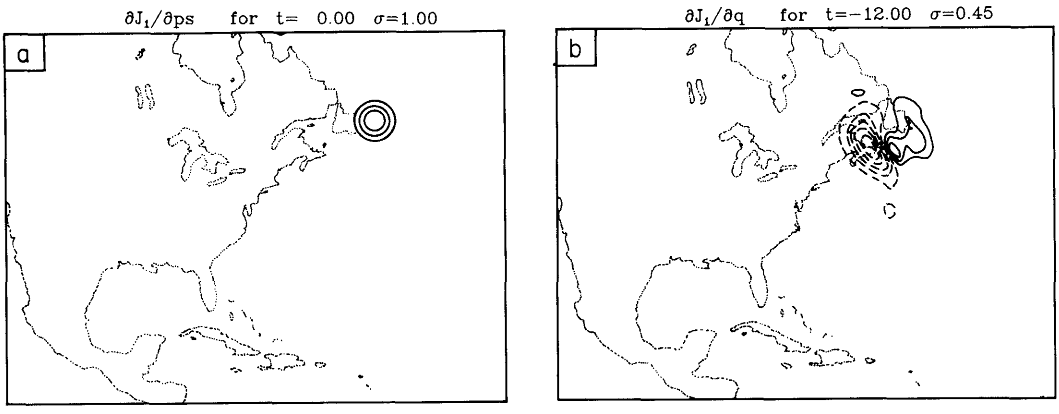

Fig. 11. Adjoint model solution for: (a) sea level pressure field at the forward model verification time (adjoint initial condition) and (b) specific humidity field at the forward model initial time (12 h prior to verification time). Both solutions are shown for the model level $\sigma = 0.45$.

perturbation (this perturbation is described in Section 3). These values are 2.162 and 1.569 when the initial perturbation has about $60\times$ larger amplitude. First we notice that the ratio of the values of ΔJ^n_{N} for the two initial perturbations is not close to 60. This itself indicates nonlinearity of the perturbation behavior in the vicinity of the cyclone as discussed in Section 3. Secondly, the relative difference between ΔJ^n_{L} and ΔJ^n_{N} is smaller for the larger initial perturbation case. This apparent contradiction is explained by the nonlinear perturbation analysis shown in Section 3. This analysis demonstrates that the evolution of small initial perturbations is dominated by forced gravity waves, unlike the larger perturbation evolution. The overall conclusion based on these results is that the ADJM for the moist diabatic MM4 version used in this study should be applied with caution. To improve moist ADJM the improvements to the moist parameterizations for the MM4 will be considered in the studies that follow.

7. Conclusions and recommendations

In this study we discuss problems related to the development and applications of an ADJM for a nonlinear model that has discontinuities in the governing equations. First we show that linearization of such a model and the evaluation of its adjoint solution are not possible formally. Then we discuss conditions that would enable construction of a satisfactory approximate TLM and ADJM for a discrete nonlinear model with discontinuous forcing functions using the reference state produced by this nonlinear model. It is assumed that the sensitivities of functions that control the regime transitions are small with respect to the small changes in the state vector that is not near the critical state for any of the given regimes.

First we study the sensitivity of regime transitions associated with the MM4 parameterizations of moist diabatic processes by performing control and perturbed nonlinear integrations for the explosive cyclogenesis synoptic case. Our results show that the regime transitions associated with the parameterized convection and related schemes are virtually insensitive to small perturbations in the initial condition unless the computational mode ($2\,\Delta t$ oscillations) is dominating the transitions. These oscillations cause highly nonlinear response of the moist tendencies to small perturbations in the state vector because the control and perturbed integrations are phase shifted by one time step. The $2\,\Delta t$ oscillations occur mainly near the explosive cyclone center where the convection and large-scale precipitation are marginal in our forecast. We conclude that the linearization of moist diabatic MM4 is feasible using the method described above, but errors may be expected in the regions where transitions are frequent and associated with large tendency changes due to moist diabatic parameterizations.

We develop the TLM and associated ADJM for the complete, moist diabatic MM4 and test the accuracy of these models. The accuracy of the TLM is evaluated first to understand the accuracy of ADJM because the accuracies of both are identical. The results presented in Section 5 show that the TLM solutions match well the nonlinear perturbation solutions everywhere in the integration domain, except in the regions where the parameterized moist diabatic processes are strongly affected by the computational mode in the nonlinear integrations. Considering this exception, we conclude that the accuracy of TLM is good even for the initial perturbation amplitudes similar to expected analysis errors. This conclusion also defines the formal accuracy of ADJM, but does not necessarily describe the expected accuracy of the results produced using the ADJM. For this purpose we also test the reliability of ADJM by performing sensitivity experiments using this model. Our results indicate that the current version of our ADJM may not be highly reliable for the explosive cyclone forecast that is used in this study or for similar cases. We would like to emphasize that this result is a consequence of modeling deficiencies of MM4 that are represented by strong effects of the computational mode upon moist diabatic processes for marginal precipitation states. To avoid this problem the improvements to the moist version of MM4 will be considered in the studies that follow.

We conclude that the TLM and associated ADJM would be more accurate, in general, for a nonlinear model that has well behaved parameterizations. We suggest that nonlinear tests similar to the experiments described in Section 3 should be performed prior to developing TLM and ADJM. If these tests show high nonlinearity for parameterized regime transitions due to the modeling deficiencies, we recommend improving the nonlinear model before performing the linearization.

8. Acknowledgments

The authors would like to thank R. Marinucci and G. Bates for providing us with the software for the regional climate model integrations. We would also like to thank K. Raeder for help in analyzing the adjoint model results. The first author is funded through NASA's Earth Observing System (EOS) Interdisciplinary Science Investigation entitled "NCAR project to interface climate modeling on global and regional scales with EOS observations." Participation at the Workshop on Adjoint Applications in Dynamic Meteorology was partially funded by NASA and the National Science Foundation.

REFERENCES

Anthes, R. A. 1977. A cumulus parameterization scheme utilizing a one-dimensional cloud model.. *Mon. Wea. Rev. 105*, 270–286.

Anthes, R. A., Hsie, E.-Y. and Kuo, Y.-H. 1987. Description of the Penn State/NCAR Mesoscale Model Version 4 (MM4). NCAR Technical Note, NCAR/TN – 282 + STR, 66 pp. [Available from the National Center for Atmospheric Research, P.O. Box 3000, Boulder, CO 80307, USA.]

Barkmeijer, J. 1992. Local error growth in a barotropic model. *Tellus 44A*, 314–323.

Bryson, A. and Ho, Y.-C. 1975. *Applied optimal control.* Hemisphere Publishing, Washington, DC, 481 pp.

Cacuci, D. G. 1981. Sensitivity theory for nonlinear systems. I: Nonlinear functional analysis approach. *J. Math. Phys. 22*, 2794–2802.

Cacuci, D. G. and Hall, M. C. G. 1984. Efficient estimation of feedback effects with application to climate models. *J. Atmos. Sci. 41*, 2063–2068.

Errico, R. M. 1990. An analysis of dynamic balance in a mesoscale model. *Mon. Wea. Rev. 118*, 558–572.

Errico, R. M. and Vukićević, T. 1992. Sensitivity analysis using an adjoint of the PSU/NCAR mesoscale model. *Mon. Wea. Rev. 120*, 1644–1660.

Errico, R. M., Vukićević, T. and Raeder, K. 1993a. Examination of the accuracy of a tangent linear model. *Tellus 45A*, 462–477.

Errico, R. M., Vukićević, T. and Raeder, K. 1993b. Comparison of initial and boundary condition sensitivity for a limited-area model. *Tellus 45A*, 539–557.

Farrell, B. F. 1990. Small error dynamics and the predictability of atmospheric flows. *J. Atmos. Sci. 47*, 2409–2416.

Giorgi, F. and Marinucci, M. R. 1991. Validation of a regional atmospheric model over Europe: Sensitivity of wintertime and summertime simulations to selected physics parameterizations and lower boundary conditions. *Q. J. R. Meteor. Soc. 117*, 1171–1206.

Hall, C. G. M., Cacuci, D. G. and Schlesinger, M. E. 1982. Sensitivity analysis of a radiative-convective model by the adjoint method. *J. Atmos. Sci. 39*, 2038–2050.

Kuo, H. L. 1974. Further studies of the parameterization of the influence of cumulus convection on large-scale flow. *J. Atmos. Sci. 31*, 1232–1240.

Kuo, Y.-H. and Low-Nam, S. 1990. Prediction of nine explosive cyclones over the Western Atlantic Ocean with a regional model. *Mon. Wea. Rev. 118*, 3–25.

Le Dimet, F. X. and Talagrand, O. 1986. Variational algorithms for analysis and assimilation of meteorological observations. Theoretical aspects. *Tellus 38A*, 97–110.

Miller, R. N., Zaron, E. D. and Bennett, A. F. 1993. Data assimilation in models with convective adjustment. *Mon. Wea. Rev.*, in press.

Smedstad, O. M. and O'Brien, J. J. 1991. Variational data assimilation and parameter estimation in an equatorial Pacific Ocean model. *Prog. Oceanog. 26*. 179–241.

Stengel, R. F. 1986. *Stochastic optimal control.* John Wiley and Sons, New York, 638 pp.

Thepaut, J.-N. and Moll, P. 1990. Variational inversion of simulated TOVS radiances using adjoint technique. *Q. J. R. Meteor. Soc. 116*, 1425–1448.

Tribbia, J. and Baumhefner, D. 1991. On the problem of prediction beyond the deterministic range. *Proc. NATO Workshop on Predictions of interannual climate variations.* Trieste, Italy, NATO/ASI Series, Springer-Verlag, 22–26 July 1991.

Tziperman, E. and Thacker, W. C. 1989. An optimal-control/adjoint-equations approach to studying the oceanic general circulation. *J. Phys. Oceanogr. 19*, 1471–1485.

Tziperman, E., Thacker, W. C., Long, R. B. and Hwang, S.-M. 1993. Oceanic data analysis using a general circulation model. Part I: Simulations. *J. Phys. Oceanogr. 22*, 1434–1457.

Verlinde, J. 1992. *Fitting microphysical observations to a numerical model through an optimal control theory technique.* Ph.D. thesis, Department of Atmospheric Sciences, Colorado State University, Fort Collins, Colorado, USA.

Vukićević, T. 1993. Possibility of skill forecast based on the finite-time dominant linear solutions for a primitive equation regional forecast model. *J. Atmos. Sci.* (April), in press.

Zou, X., Navon, I. M. and Le Dimet, F. X. 1992. Incomplete observations and control of gravity waves in variational data assimilation. *Tellus 44A*, 273–298.

Zou, X., Navon, I. M. and Sela, J. G. 1993. Variational data assimilation with moist threshold processes using NMC spectral model. *Tellus 45A*, 370–387.

Županski, D. 1993. The effect of discontinuities in the Betts-Miller cumulus convection scheme on four dimensional data assimilation. *Tellus 45A*, 511–524.